A thermal spike model of grain growth under irradiation

D. Kaoumi,[1,a)] A. T. Motta,[1] and R. C. Birtcher[2]
[1]*Department of Mechanical and Nuclear Engineering, The Pennsylvania State University, 227 Reber Bldg., Pennsylvania 16802, USA*
[2]*Materials Science Division, Argonne National Laboratory, Bldg. 212, Illinois 60540, USA*

(Received 11 April 2008; accepted 7 August 2008; published online 8 October 2008)

The experimental study of grain growth in nanocrystalline metallic foils under ion irradiation showed the existence of a low-temperature regime (below about $0.15-0.22T_m$), where grain growth is independent of the irradiation temperature, and a thermally assisted regime where grain growth is enhanced with increasing irradiation temperature. A model is proposed to describe grain growth under irradiation in the temperature-independent regime, based on the direct impact of the thermal spikes on grain boundaries. In the model, grain-boundary migration occurs by atomic jumps, within the thermal spikes, biased by the local grain-boundary curvature driving. The jumps in the spike are calculated based on Vineyard's analysis of thermal spikes and activated processes using a spherical geometry for the spike. The model incorporates cascade structure features such as subcascade formation, and the probability of subcascades occurring at grain boundaries. This results in a power law expression relating the average grain size with the ion dose with an exponent equal to 3, in agreement with the experimental observations. The model is applied to grain growth observed *in situ* in a transmission electron microscope in a wide range of doses, temperature, and irradiation conditions for four different pure metals, and shown to predict well the results in all applicable cases. Some discussions are also presented on the expansion of the model to the thermally assisted regime. The paper is organized in six sections. Section I gives background and literature review, while Secs. II and III review experimental methods and results for *in situ* grain growth under irradiation. Section IV derives the model proposed to find the grain-growth equation in the nonthermal regime, and in Sec. V the model is applied to the results. In Sec. VI grain growth in the thermally assisted regime is discussed and Sec. VII presents the conclusions. © *2008 American Institute of Physics*. [DOI: 10.1063/1.2988142]

I. BACKGROUND

Grain growth under irradiation is a phenomenon of interest to several applications, including the behavior of materials in nuclear reactors and the behavior of thin-film solid state devices that are modified by ion implantation.[1–10] In particular, several researchers have investigated grain growth in thin films under ion irradiation. In a study of ion-irradiated Ni thin films, Wang *et al.*[1,11] observed that grain diameter increased linearly with dose and that the grain-boundary mobility increased linearly with deposited damage energy. Atwater *et al.*[8] studied ion-induced grain growth in Au, Ge, and Si thin films, finding that the grain size D increased with dose (Φt) according to $D^n \propto \Phi t$ with $1.96 < n < 4$. They reported a weak dependence of ion-irradiation-induced grain growth on temperature, with activation energies on the order of 0.15 eV for Ge films irradiated in the temperature range of 723–973 K and less than 0.1 eV for Si films irradiated between 1023 and 1123 K. An atomistic model was proposed to describe ion enhanced grain growth based on vacancy formation and jumps across the boundary. The model was ballistic in nature and resulted in a linear dependence of mobility on the defect generation rate, i.e., on the linear deposited damage energy per ion F_D (which did not correspond to experimental observations).

In another study of ion-induced grain growth Liu and co-workers worked on a series of pure metal thin films and coevaporated alloy systems of Ni–Co, Ni–Cu, and Pd–Pt, and found that the grain size increased with dose, with an exponent near 3.[6,7] Liu *et al.*[7] mentioned a saturation effect on grain size and suggested that the saturation grain size could be related to the size of the defect cascade generated by a single ion. However, no theoretical derivation was given to support this conjecture. Liu identified two temperature regimes of ion-induced grain growth in Cu, the first being independent of temperature below 213 K, and the second showing a temperature dependence, with an activation energy of 0.14 eV above 213 K. Also, the observation of significant variations in grain-growth rates among systems that exhibit similar collisional damage behavior (such as Ni–Cu alloys of different atomic concentrations) showed that a purely ballistic model was inadequate for describing ion-induced grain growth; this led the authors to conclude that intrinsic material properties must be taken into account when modeling ion-induced grain growth. The authors suggested that ion-irradiation-induced grain growth may be related to the "thermal spike" created during ion irradiation. The mobility of grain boundaries was related to the number of atomic jumps generated in a thermal spike expressed in Vineyard's analysis of thermal spikes.[12,13] Furthermore, it was observed that greater grain growth was induced in materials with low cohesive energy ΔH_{coh}, which was explained

a)Electronic mail: kaoumi@psu.edu.

by assuming that the activation energy for atomic jumps scales with the cohesive energy.[14] Assuming a cylindrical geometry for thermal spikes, it was proposed that the mobility of grain boundaries scales with $F_D^2/\Delta H_{coh}^2$, where F_D is the deposited damage energy linear density.

Alexander and co-workers[2–4] used the proposed thermal spike approach of Liu and derived a model of ion-induced grain growth in their study of the ion-irradiated binary systems Ni–Al, Pt–Ti, Pt–V, Pt–Ni, and Au–Co. Their experimental results showed normal grain growth in all their films studied with the average grain size increasing with ion dose according to $\bar{D}^n - \bar{D}_0^n = K(\Phi t)$, with n ranging from 1.9 to 4.3 (average $n=3$). The thermal spike model of ion-irradiation grain growth developed by Alexander incorporated grain-boundary curvature and chemical gradients as the driving forces for atomic migration across boundaries within the thermal spikes. The model considered cylindrical thermal spikes along the path of the ion of linear energy density F_D, which was taken as the average energy deposited in nuclear interactions per unit length obtained from TRIM. Alexander and Was[15] acknowledged that their thermal spike model of grain growth under ion irradiation was an idealized picture, especially since it did not take into account the nature of the cascade structure (subcascade formation), which is expected to vary considerably among different ion-target combinations. Their theoretical model yielded a grain-boundary mobility proportional to $F_D^2/\Delta H_{coh}^3$ in contrast with $F_D^2/\Delta H_{coh}^2$ proposed by Liu, and a grain-growth exponent of 2. The authors associated the experimental deviations from ideal parabolic ($n=2$) grain-growth kinetics with the drag effect of inhibiting driving forces such as solute drag.

Thus, although several studies of grain growth under irradiation have been made and various models were proposed, the observed kinetics of grain growth with the exponent around 3 have not been explained by the existing models.

This study develops a theory of grain growth under ion irradiation based on the incidence of thermal spikes at grain boundaries, and addresses the discrepancies mentioned above by taking fuller account of the cascade structure and grain geometry. Also, since the model is applied to experimental results obtained on nanocrystalline metals, this study also provides insight on the stability of nanocrystalline materials under irradiation, for which information is lacking as pointed out in the reviews of the field.[16–18]

II. EXPERIMENTAL METHODS

A. Materials and sample preparation

Details about the materials and sample preparation are given in Ref. 19 and are briefly reviewed here. Elemental thin films of Zr, Cu, Pt, and Au, and supersaturated solid solutions of Zr–Fe and Cu–Fe were (co)sputter deposited onto NaCl substrates using a dual gun system at a base pressure of less than 10^{-6} Torr at room temperature at the Materials Research Laboratory (Penn State University). The coated NaCl substrates were then cleaved into small pieces and the specimens were floated on a de-ionized water-ethanol solution onto transmission electron microscope (TEM) copper grids, cleaned in de-ionized water, and dried before they were used for the irradiations.

The four pure elements were chosen to independently investigate the role of collisional processes and melting temperature: on grain growth: Pt and Zr have similar melting points but very different atomic masses (i.e., different recoil spectra); and the same is true for Au and Cu. On the other hand, Pt and Au are adjacent elements in the periodic table of elements and should therefore exhibit similar recoil spectra under the same irradiation conditions, but the two elements have very different melting points. Hence comparing results for Au and Pt should highlight the effect of melting temperature (and properties which scale with it) on the grain-growth process.

B. Microstructure of as-deposited films

The as-deposited films were 80–90 nm thick, laterally homogeneous, and nanocrystalline, with an initial average grain size between 10 and 15 nm, with a roughly equiaxed grain microstructure. The diffraction patterns (DPs) of the as-deposited films were characteristic of Cu, Au, Pt, and Zr respectively, with the expected fcc crystal structures (hcp in the case of Zr) and with lattice parameters equal those of the bulk materials. For the Zr–Fe solid solutions only the DPs of hcp-Zr were observed.[19]

C. Irradiation experiments

The ion irradiations were conducted at the intermediate voltage electron microscope (IVEM)-Tandem facility at Argonne National Laboratory, where an ion accelerator is attached to an electron microscope operated at 300 keV[20] so that the grain growth (and the qualitative evolution of grain morphology) could be followed *in situ* on the microscope. Samples were irradiated with 500 keV Ar and Kr ions, 600 keV Ar and Kr ions, and with 1 MeV Kr ions at different temperatures ranging from 20 to 573 K. The ion-beam energy was chosen on the basis of computer simulations using the Monte Carlo program SRIM2003 so as to minimize ion implantation while maximizing the deposited damage energy.[21] The energy of the ions was such that most ions pass through the samples for the different cases (typically between 84% and 98%, except for the case of the 900 Å thick Cu foils irradiated with 500 keV Kr ions, where 67% of the ions pass through). Ion fluxes were typically around 2.50×10^{12} ions/cm^2 s. The irradiation conditions such as the displacement rate, irradiation temperature, ion type and energy, melting points of the materials, and the collisional properties (displacement rate and deposited damage energy F_D) are summarized in Table I.

The evolution of the microstructure was followed by sequentially taking bright-field images and DPs of the films during irradiation. This made it possible to follow the kinetics of the irradiation-induced phenomena.

III. SUMMARY OF EXPERIMENTAL RESULTS

The main experimental results previously reported in Refs. 10 and 19 are summarized below:

TABLE I. Summary of the irradiation conditions: melting points, temperatures of irradiation, ion type, and energy. The collisional properties (displacement rate and deposited damage energy F_D) were calculated using the SRIM2003[21] Monte Carlo code using a displacement energy of 25 eV/at.

Element	Melting point (K)	Ion type/energy	Damage energy deposited (F_D)(eV/ion Å)	Displacement cross-section (displacement/ion Å)	Displacement rate (dpa/s)	Irradiation temperature (K)
Au	1337	Ar 500 keV	100	2.83	0.012	50, 298, 473
Pt	2041	Ar 500 keV	120	3.50	0.013	298
		Kr 1 MeV	367	9.78	0.018	50, 298, 473, 773
Cu	1358	Kr 500 keV	323	7.91	0.023	50, 298, 573
Zr	2128	Kr 500 keV	194	3.67	0.021	20
Ze–Fe	2128	Kr 500 keV	194	3.67	0.021	20, 298, 423, 573

(1) *Grain growth under irradiation occurs at all temperatures studied.* All samples studied showed a gradual increase in the grain size with ion dose at all temperatures, even at temperatures down to 20 K. Figure 1 shows a bright-field sequence of the evolution of thin films of Au, Pt, and Cu at various fluences when irradiated at room temperature. It is clear that grain growth occurs and that it varies from material to material. Grain growth also occurs under purely thermal conditions if the temperature is high enough but is slower than under irradiation and it requires a higher irradiation temperature (this limit was not exactly determined in this study, but it is likely above 0.3 T_m).

(2) Similarly to ion-beam-mixing, *ion-irradiation-induced grain-growth exhibits three different regimes with respect to irradiating temperature:*

(i) a purely thermal regime where thermal effects dominate the grain-growth process,

(ii) a thermally assisted regime where thermal motion and irradiation effects combine to increase the rate of grain growth caused by either of these mechanisms operating alone, and

(iii) a low-temperature (or "nonthermal") regime in which irradiation effects dominate the grain-growth process and the kinetics do not depend on the irradiating temperature.

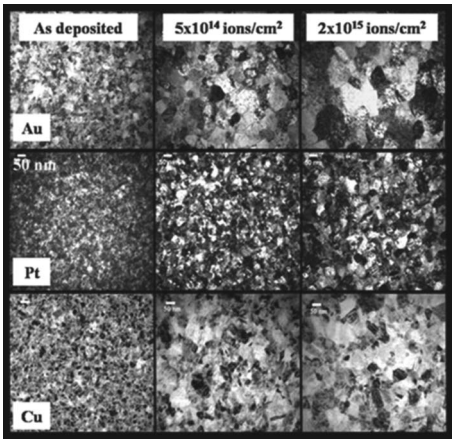

FIG. 1. Sequence of bright-field TEM images taken at different ion doses showing grain-growth induced by ion irradiation at room temperature; from left to right: as deposited, 5×10^{14} ions/cm^2, 2×10^{15} ions/cm^2; from top to bottom: pure Au thin-film irradiated with 500 keV Ar ions, Pt irradiated with 500 keV Ar ions, and Cu irradiated with 500 keV Kr ions.

The transition temperature between the nonthermal and thermally assisted regimes depends on the material but can be scaled with its melting temperature; it occurrs at a homologous temperature between 0.15 and 0.20 T_m.

(3) *The average grain size follows an exponential law with fluence with* $n\sim3$: grain size was measured from the micrographs and plotted versus ion dose. Details about the grain size measurements and the grain-growth curve fittings are provided in Ref. 19. The grain-growth curves revealed a common trend for all compositions considered and for all irradiating temperatures (some of these curves are shown at the end of this article when the model is compared to the experimental data.) Similarly to the relationship between the average grain size (D) and annealing time (t) in the case of thermally induced grain growth,[22,23] ion-irradiation induced grain-growth curves can be fitted with the expression: $D^n-D_0^n=K(\Phi t)$, where D_0 is the initial mean grain diameter, Φ is the ion flux, t is the exposure time, n is a constant, and K is a constant that depends on the grain-boundary mobility and the driving force. The fitting parameters (K,n) varied depending on the material and the temperature. As can be seen in Table II, values of n between 2.5 and 3.5 (average value of 3) were found, revealing a slower grain growth than that predicted by Hillert's[24] model of thermal grain growth driven by grain curvature in conventional polycrystalline materials, for which $n=2$.

(4) *Grain growth did not occur under 1 MeV electron irradiation up to high doses:* electron irradiation of Zr based thin films to 180 dpa (displacements per atom) showed no increase in grain size. We interpret this result to mean that a minimum local density of defects (such as formed in the cascades created by ion irradiation) is needed for grain growth to occur. This indicates that only defects created within dense subcascades (i.e., thermal spikes) influence grain-growth kinetics.

To account for the experimental observations above, we propose a model for grain growth under irradiation in the low-temperature regime ("temperature-independent regime"), based on the presence of thermal spikes.

TABLE II. Summary of the fitting parameters.

Irradiation conditions			Fit parameters			
Element	Ion type/Energy	Temperature (K)	D_0 (nm)	n	K (nm^n/dpa)	Coefficient of determination R^2 (%)
Zr	Kr/500 keV	20	14.17	2.74	0.41×10^3	99.7
Au	Ar/500 keV	50	9.24	2.91	16.6×10^3	91.3
		298	13.2	2.68	12.2×10^3	97.3
		473	25.53	3.00	1.86×10^5	91.3
Cu	Kr/500 keV	50	12.30	3.30	2.91×10^3	99.1
		298	13.6	3.17	4.15×10^3	99.6
		573	73.69	3.51	1.53×10^{10}	98.0
Pt	Kr/1 MeV	50	12.36	3.12	7.36×10^3	97.5
	Kr/1 MeV	298	14.5	3.27	12.4×10^3	99.0
	Ar/500 keV	298	12.0	2.97	4.15×10^3	99.0
	Kr/1 MeV	773	20.22	3.25	4.10×10^4	99.1

IV. THERMAL SPIKE MODEL OF GRAIN GROWTH UNDER IRRADIATION

A. Driving force for grain-boundary migration and assumptions

The driving force for grain-boundary migration is the curvature of the grain boundary. A curved grain boundary is subject to a pressure (i.e., force per unit area of grain boundary) of magnitude:

$$P_{\text{curv}} = \frac{2\gamma}{R}, \tag{1}$$

where γ is the grain-boundary surface energy per unit area of grain boundary, R is the radius of curvature of the grain boundary, which for a spherical grain is equal to the grain radius. Under purely thermal conditions the atomic jumps across the grain boundary are biased in favor of reducing the grain-boundary curvature, which results in the growth of some grains at the expense of others. Ion-irradiation-induced grain growth is subject to the same driving force as thermal grain growth, but the atomic transport mechanisms are different.

The idea behind the thermal spike model of ion-irradiation-induced grain growth is as follows. After the collisional phase of a displacement cascade, the remaining kinetic energy of the recoil atoms is thermalized within the crystal lattice. The result is a short lived "temperature spike" in a very localized region. This spike will be more or less large depending on the energy of the recoil and the properties of the material. If the spike occurs in the direct vicinity of a grain boundary, atoms which are thermally activated within the thermal spike region can jump across the boundary. The local driving forces present (e.g., chemical concentration gradients and grain-boundary curvature) then cause the net number of atom jumps to be in the direction of reducing grain-boundary curvature and, as a result, the boundary migrates in the opposite direction. Two important assumptions underlie the model proposed to describe grain growth under ion irradiation in the low-temperature regime.

Assumption 1: Only defects created in the direct vicinity of grain boundaries contribute to grain growth.

This assumption is supported by the observation that grain growth does not depend on substrate temperature in this regime, which implies that long-range thermal diffusion is not significant. Rate theory calculations also support this assumption in this low-temperature regime. The defects created by irradiation are continuously eliminated by reacting with other defects and with defect sinks. Depending on the displacement rate, the temperature, sink strengths, the majority of the defects can be eliminated by recombination ("recombination-dominated regime") or by absorption at sinks ("sink-dominated regime"). As will be seen below, our experiments are in the recombination-dominated regime, i.e., typical diffusion length is smaller than the average grain size, which supports the assumption above.

To evaluate which regime is operational (sink dominated or recombination dominated) the E parameter, defined in Eq. (2), is estimated. E is defined as

$$E = \frac{4K_0K_{iv}}{\left(\sum_s k_{\text{is}}^2 D_i\right)\left(\sum_s k_{\text{vs}}^2 D_v\right)}, \tag{2}$$

where K_0 is the displacement rate (in dpa), K_{iv} is the rate constant for interstitial-vacancy recombination and is defined as follows:

$$K_{iv} = \frac{4\pi r_{iv}(D_i + D_v)}{V_{\text{at}}} = K_{iv_0}(D_i + D_v), \tag{3}$$

where V_{at} is the atomic volume, D_v and D_i are the diffusion coefficients for vacancies and interstitials, respectively, and r_{iv} is the radius of the recombination volume. k_{is}^2 and k_{vs}^2 [in Eq. (2)] are the sink strengths for interstitial and vacancy absorption into sink s. In fact, the parameter E compares the defect losses to vacancy-interstitial recombination [numerator in Eq. (2)] with the defect losses to fixed sinks such as voids, dislocations, grain boundaries, and free surfaces (denominator). A value of $E \ll 1$ indicates operation in a sink-dominated regime, whereas $E \gg 1$ indicates operation in a recombination-dominated regime. The details of the calculation of the E parameter are given in the Appendix. The value of E was computed versus irradiation temperature for the different systems: Au irradiated with 500 keV Ar ions, Cu/500 keV Kr, Pt/1 MeV Kr, and Zr/500 keV Kr and is plotted in Fig. 2. The curves obtained in Fig. 2 clearly indicate that, at the temperatures of interest, $E \gg 1$, thus the system is op-

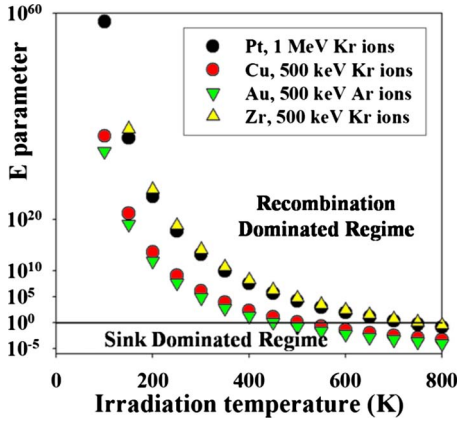

FIG. 2. (Color online) E parameter (logarithmic scale) vs irradiation temperature for Au irradiated with 500 keV Ar ions, Pt irradiated with 1 MeV Kr ions, Zr irradiated with 500 keV Kr ions, and Cu irradiated with 500 keV Kr ions.

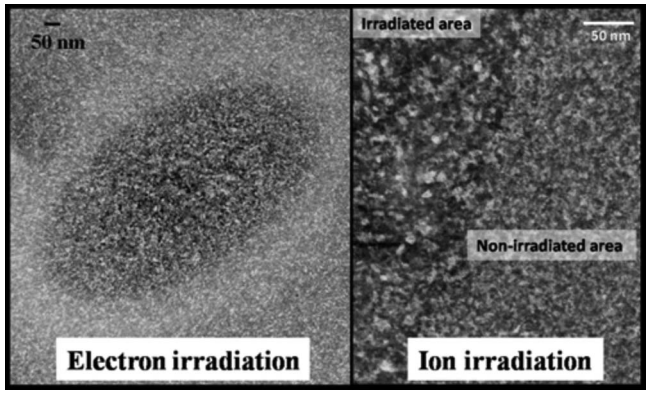

FIG. 3. (Left) Bright-field image of a Zr–Fe thin film irradiated with 1 MeV electron irradiation to a dose of 80 dpa at room temperature. (Right) Zr–Fe thin film irradiated with 600 keV Kr ions to 10^{16} ions/cm^2 ($\sim$75 dpa) at room temperature. The ion irradiation has induced grain growth while the electron irradiation has not.

erating in the recombination-dominated regime. This is true even though E was computed for the initial conditions, when the grain-boundary sink strength is the highest (when the grains grow the grain-boundary density decreases). At these temperatures the diffusion length is shorter than the recombination radius, supporting the idea that only defects created in the direct vicinity of the grain boundary participate in grain growth.

Assumption 1 is also supported by computer simulations from Voegeli *et al.*[25] who used molecular dynamics (MD) to simulate 5 keV cascades in nanocrystalline-Ni samples and found that ion-induced grain growth is observed only if the thermal spike volume is larger than the grain volume or overlaps the grain-boundary area. If the spike volume does not reach the grain-boundary area, ion-induced grain growth is not observed. By the way, this result implicitly also supports the idea of a cascade size effect on the kinetics of ion-irradiation-induced grain growth.

Assumption 2: Isolated displacements resulting from elastic collisions do not contribute to grain growth.

This assumption stems from the observation that no grain growth was observed during 1 MeV electron irradiation of the Zr–Fe thin films, as shown in Fig. 3, which compares bright-field images of Zr–Fe foils irradiated at room temperature to 80 dpa under electron irradiation (left image) and 75 dpa under 600 keV Kr ion irradiation (right image). In each case a nonirradiated area of the sample could be compared to the irradiated area to determine whether grain growth occurred as a result of the irradiation. In the case of electron irradiation, the outline of the electron beam is clearly visible in the image, and no grain growth occurred in the irradiated area with respect to the nonirradiated area, whereas in the case of ion irradiation for a similar dose (in terms of dpa), grain growth clearly occurred in the irradiated area.

The main difference between the two types of irradiation is that in the case of electron irradiation, the displacements are homogeneously created, without cascades and therefore without thermal spikes. This shows that there is a need for a local density of defects for grain growth to occur, hence Assumption 2.

In summary, in the low-temperature regime, ion-irradiation grain growth is caused by the thermal spikes intersecting grain boundaries.

B. Derivation of the grain-growth rate equation

As an ion interacts with matter, primary knock-on atoms (PKA) are displaced from their lattice sites with some kinetic energy. The PKAs (of high enough energy) subsequently dissipate their energy through displacement (sub)cascades, which result in local thermal spikes. Some of these spikes occur within the bulk of grains, others hit near grain boundaries as illustrated in Fig. 4, which shows a schematic representation of the cascade structure induced by an ion transversing a polycrystalline thin film. Based on the assumptions enunciated above, only the spikes occurring at grain boundaries participate in grain-boundary migration hence grain growth.

Based on this picture, the following analytical model is derived to account for the grain-growth kinetics of the *average grain* assumed to be spherical. If χ is the average number of thermal spikes triggered by one ion per unit depth in the thin film, then the number of spikes per unit time and per unit volume of material when nonoverlapping cascades are assumed is given by

$$\Phi[\text{ions s}^{-1}\ \text{cm}^{-2}]\chi[\text{spikes ion}^{-1}\ \text{cm}^{-1}], \quad (4)$$

where Φ is the ion flux. The rate of spikes per unit volume occurring at the grain boundary is

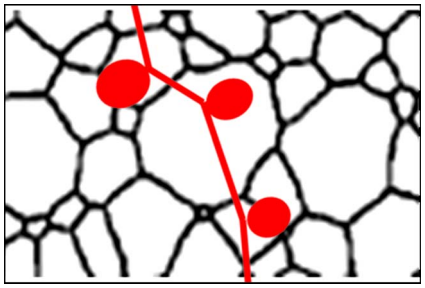

FIG. 4. (Color online) Schematic representation of the cascade structure induced by an ion transversing a polycrystalline thin film.

$$\Phi\chi f_{GB}, \tag{5}$$

where f_{GB} is the fraction of spikes intersecting the grain boundary. The total number of spikes occurring at the grain boundary per unit time is

$$\Phi\chi f_{GB} V_{GB}, \tag{6}$$

where V_{GB} is the volume associated with the grain boundary. When a thermal spike occurs at a grain boundary the atomic jumps within the spike are biased by the local curvature of the grain boundary (i.e., the local driving force for grain-boundary migration) such that a net number of jumps across the grain boundary occurs in the direction reducing the curvature. If η is the integrated number of atomic jumps over the lifetime of a thermal spike occurring at the grain boundary (under the influence of the local grain-boundary curvature), the total net number of atomic jumps across the grain boundary is given by

$$\Phi\chi f_{GB} V_{GB}\eta. \tag{7}$$

Equation (7) gives the net number of atomic jumps involved in grain-boundary migration (and hence in grain growth). Each atomic jump increases the volume of the grain by the atomic volume V_{at}. Hence, after a dose increment $\Delta(\Phi t)$, the volume of the average grain increases by

$$\Delta V = \Delta(\Phi t)\chi f_{GB} V_{GB}\eta V_{at}. \tag{8}$$

Therefore the grain volume increase per unit dose is given by

$$\frac{\Delta V}{\Delta(\Phi t)} = \chi f_{GB} V_{GB}\eta V_{at}. \tag{9}$$

If the ion flux Φ is constant, Eq. (9) becomes

$$\frac{\Delta V}{\Delta t} = \Phi\chi f_{GB} V_{GB}\eta V_{at} \approx \frac{dV}{dt}. \tag{10}$$

Equation (10) gives the expression of the grain-growth rate in terms of volume.

For the average grain modeled as a sphere of diameter D,

$$V_{GB} = \pi D^2(\delta/2), \tag{11}$$

where $\delta/2$ is the width in the grain associated with the grain boundary. The change in volume of the average grain can also be expressed as

$$\frac{dV}{dt} = \frac{d\left(\frac{\pi D^3}{6}\right)}{dt} = \frac{\pi D^2}{2}\frac{dD}{dt}. \tag{12}$$

Setting Eq. (10) equal to Eq. (12) leads to

$$\frac{\pi D^2}{2}\frac{dD}{dt} = \pi D^2\frac{\delta}{2}\Phi\chi f_{GB}\eta V_{at}, \tag{13}$$

which simplifies into

$$\frac{dD}{dt} = \delta\Phi\chi f_{GB}\eta V_{at}. \tag{14}$$

Equation (14) is the fundamental equation determining the kinetics of ion-irradiation-induced grain growth in the temperature-independent regime. We now evaluate the terms of Eq. (14).

C. The f_{GB} term

The fraction of spikes intersecting the grain boundary f_{GB} is defined as the fraction of atomic sites close enough to the grain boundary such that if a thermal spike is induced locally it intersects the grain boundary. Assuming a spherical shape for the average grain and spike, f_{GB} is the fraction of sites within a distance equal to the spike radius from the grain boundary and is written as

$$f_{GB} = \frac{\pi D^2\frac{d_{spike}}{2}}{\frac{\pi D^3}{6}} = \frac{3d_{spike}}{D}, \tag{15}$$

where D and d_{spike} are the diameter of the average grain and the average thermal spike, respectively. f_{GB} decreases with increasing D reflecting the fact that as grains grow, the probability of thermal spikes occurring at the grain boundary decreases.

D. The number of displacements (η) induced in a thermal spike of energy Q

The determination of the number of jumps (η) induced in a thermal spike of energy Q is based on Vineyard's analysis of thermal spikes and activated processes.[12] This analysis is based on the assumption that energy is deposited in a very small region, producing a localized increase in temperature that spreads and cools according to the laws of classical heat conduction in a homogeneous continuum. If an activated process (e.g., migration of atoms) is energized by the spike, then the number of elementary steps (e.g., atomic jumps) caused by one spike can be expressed as the integral over space and time of the atomic jump rate in the spike.

1. Thermal spike in an infinite medium under no driving force

We assume that the energy of a thermal spike Q is that of the initial recoil atom (PKA). If we consider that the energy of the spike is introduced at a point in the medium with an initial deposited energy distribution of $Q\delta^3(r)$ where $\delta^3(r)$ is the three-dimensional (3D) delta function, the subsequent dissipation of this energy results in a temperature distribution $T(r,t)$ in the thermal spike region. Since MD studies show that a spherical geometry would be appropriate to describe cascades and subcascades, a spherical cascade is assumed here. Vineyard derived an expression for $T(r,t)$ by solving the heat conduction equation in spherical geometry, assuming a simple power law dependence on temperature for the thermal conductivity κ, and the heat capacity c such that

$$\kappa = \kappa_0 T^{n-1} \quad \text{and} \quad c = c_0 T^{n-1} \quad \text{with} \quad n \geq 1. \tag{16}$$

where κ_0 and c_0 are the values of the thermal conductivity and the heat capacity at ambient temperature respectively.

The time-dependent solution for the temperature distribution is given by[12]

$$T(r,t) = \left(\frac{nQc_0^{1/2}}{(4\pi\kappa_0 t)^{3/2}}\right)^{1/n} \exp\left(-\frac{c_0 r^2}{4n\kappa_0 t}\right). \quad (17)$$

It should be noted that in such a treatment, the target macroscopic temperature or "ambient temperature" is taken as absolute zero. If the ambient temperature is not zero, the integration of the equations cannot be achieved analytically.

According to Vineyard, atomic motion within the spike is promoted thermally and these thermally activated atomic jumps are assumed to obey a directionally random Arhenius law such that the jump rate is given by[12]

$$R(r,t) = A \exp\left(-\frac{E_a}{k_B T(r,t)}\right), \quad (18)$$

where E_a is the activation energy for atomic jump in the thermal spike, k_B is Boltzmann's constant, and A is a constant independent of temperature. Hence the total number of $T(r,t)$ is the temperature distribution within the spike. Hence the total number of atomic jumps induced in one thermal spike η is obtained by substituting $T(r,t)$ from Eq. (17) into Eq. (18) and integrating over time and space according to

$$\eta = \int_0^\infty dV \int_0^\infty R(r,t)dt \quad (19)$$

where dV is the infinitesimal volume and $R(r,t)$ is the atomic jump rate per unit volume. In the absence of driving forces, and if the spike is assumed spherical then η is expressed as

$$\eta = \int_0^\infty 4\pi r^2 dr \int_0^\infty A \exp\left(-\frac{E_a}{k_B T(r,t)}\right)dt. \quad (20)$$

The integration of Eq. (20) is done by changing variables and the total number of atomic jumps occurring in a thermal spike of energy Q, as it develops and cools, is[12]

$$\eta = \frac{\sqrt{\frac{3}{5}} A n^{8/3} Q^{5/3}}{10\pi C_0^{2/3}\kappa_0}\left(\frac{k_B}{E_a}\right)^{(5n/3)} \Gamma\left(\frac{5n}{3}\right), \quad (21)$$

where $\Gamma(5n/3)$ is the gamma function of argument $5n/3$. However, Eq. (21) does not take into account the effect of local driving force on the atomic jumps. Indeed, the $R(r,t)$ expression in Eq. (18) is for random jumps and does not include the biasing effects of local driving forces (i.e., chemical potential gradients) on atomic migration within the spike if the spike occurs in the direct vicinity of a grain boundary for instance. The local chemical potential gradients should be incorporated in $R(r,t)$,[2] as shown in Sec. IV D 2 for the case of a spherical thermal spike.

2. Incorporating the driving force due to grain-boundary curvature

Here we are considering a thermal spike occurring at a grain boundary where the atomic jumps within the spike are biased by the local driving force due to the grain-boundary curvature. The net rate of atomic jumps across the grain-boundary $R(r,t)$ is first obtained in the case of grain-boundary migration occurring under typical isothermal annealing conditions (i.e., steady-state and uniform temperature T), i.e., $R(r,t)=R$ using classical results on thermally activated grain-boundary migration.[12] R is given by

$$R_{\text{net}} = \nu \exp\left(-\frac{E_a}{k_B T}\right)\left[1 - \exp\left(-\frac{\Delta G_{\text{curv}}}{k_B T}\right)\right], \quad (22)$$

where ν is a frequency term per atom; E_a is the energy barrier that an atom needs to overcome to break away from a site and jump to another site; E_a is the sum of the activation energy for vacancy formation and the activation energy for vacancy migration. ΔG_{curv} is the free energy difference across the grain boundary due to its curvature.

Since $\Delta G_{\text{curv}} \ll k_B T$, the following approximation follows:

$$\exp\left(-\frac{\Delta G_{\text{curv}}}{k_B T}\right) \approx 1 - \frac{\Delta G_{\text{curv}}}{k_B T}, \quad (23)$$

and Eq. (22) can be written as

$$R_{\text{net}} = \frac{\Delta G_{\text{curv}}}{k_B T}\nu \exp\left(-\frac{E_a}{k_B T}\right). \quad (24)$$

In the case of a thermal spike occurring at a grain boundary, the net rate of atomic jumps across the grain boundary per unit volume $R(r,t)$ within the thermal spike is obtained by substituting the temperature distribution within the spike $T(r,t)$ in Eq. (24) and multiplying by the atomic density to obtain the number of atomic jumps per unit volume,

$$R(r,t) = N_{\text{at}}\nu\frac{\Delta G_{\text{curv}}}{k_B T(r,t)}\exp\left(-\frac{E_a}{k_B T(r,t)}\right). \quad (25)$$

The local chemical potential gradient ΔG_{curv} due to grain-boundary curvature, which corresponds to P_{curv} in Eq. (1), can be written as

$$\Delta G_{\text{curv}} = \frac{4\gamma V_{\text{at}}}{D}, \quad (26)$$

where ΔG_{curv} is in units of J at.$^{-1}$, the atomic volume V_{at} is in m^3 at.$^{-1}$, the grain-boundary surface energy γ is in J m^{-2}, and the average grain size (or diameter) D is in m. Equation (26) can be incorporated in Eq. (25) which then becomes

$$R(r,t) = \frac{4\gamma V_{\text{at}}}{D k_B T(r,t)} N_{\text{at}}\nu \exp\left(-\frac{E_a}{k_B T(r,t)}\right). \quad (27)$$

The total number of jumps within the thermal spike is then given by the integral

$$\eta_{\text{curv}} = \int_0^\infty 4\pi r^2 dr \int_0^\infty \frac{4\gamma V_{\text{at}} N_{\text{at}}}{D k_B T(r,t)}\nu \exp\left(-\frac{E_a}{k_B T(r,t)}\right)dt. \quad (28)$$

Using Eq. (17) for $T(r,t)$, the integration of Eq. (28) is done by change of variables and gives

$$\eta_{\text{curv}} = \frac{4\gamma V_{\text{at}} N_{\text{at}} \nu}{D k_B} \frac{\sqrt{\frac{3}{5}} n^{8/3} Q^{5/3}}{10\pi C_0^{2/3} \kappa_0} \left(\frac{k_B}{E_a}\right)^{[(5n/3)+1]} \Gamma\left(\frac{5n}{3}+1\right) \tag{29}$$

If $n=1$ (i.e., if the heat capacity and heat conductivity are assumed constant within the spike), η_{curv} becomes

$$\eta_{\text{curv}} = \frac{4\gamma V_{\text{at}} N_{\text{at}} \nu}{D k_B} \frac{\sqrt{\frac{3}{5}} \Gamma\left(\frac{8}{3}\right) k_B^{8/3}}{10\pi C_0^{2/3} \kappa_0} \frac{Q^{5/3}}{E_a^{8/3}}. \tag{30}$$

It is noted that according to Ref. 14 the activation energy E_a for atomic jump can be scaled with the cohesive energy of the material according to

$$E_a = \beta \Delta H_{\text{coh}}. \tag{31}$$

As a result, η_{curv} is proportional to $Q^{5/3}/\Delta H_{\text{coh}}^{8/3}$ where Q is the PKA energy.

E. The grain-growth equation

Finally, by incorporating Eqs. (15) and (30) into Eq. (14), the grain-growth rate becomes

$$\frac{dD}{dt} = \frac{\Phi \chi \delta}{N_{\text{at}}} \frac{3 d_{\text{cas}}}{D} \left[\frac{4\gamma V_{\text{at}} N_{\text{at}} \nu}{D k_B} \frac{\sqrt{\frac{3}{5}} \Gamma\left(\frac{8}{3}\right) k_B^{8/3}}{10\pi C_0^{2/3} \kappa_0} \frac{Q^{5/3}}{E_a^{8/3}} \right]. \tag{32}$$

Equation (32) relates the time evolution of the average grain size with material properties (such as the specific heat, the thermal conductivity, the atomic volume, the Debye frequency, the grain-boundary energy, and the cohesive energy) with irradiation parameters (such as the ion flux, the average spike energy and size, and the number of thermal spikes induced by the ions). It can thus rationalize the differences in grain-growth kinetics observed in materials with similar collisional properties but different material properties. The variables D and t can be separated in Eq. (32) which is rewritten as

$$D^2 dD = \left[12\gamma d_{\text{spike}} \Phi \chi \delta \frac{V_{\text{at}} \nu \sqrt{\frac{3}{5}} \Gamma\left(\frac{8}{3}\right) k_B^{5/3}}{10\pi C_0^{2/3} \kappa_0} \frac{Q^{5/3}}{E_a^{8/3}} \right] dt. \tag{33}$$

Finally, the grain-growth equation for the thermal spike model is obtained by integrating Eq. (33) from an initial size D_0 to a final size D

$$D^3 - D_0^3 = \left[36\gamma d_{\text{spikes}} \chi \delta \frac{V_{\text{at}} \nu \sqrt{\frac{3}{5}} \Gamma\left(\frac{8}{3}\right) k_B^{5/3}}{10\pi C_0^{2/3} \kappa_0} \frac{Q^{5/3}}{E_a^{8/3}} \right] \Phi t = K \Phi t. \tag{34}$$

Equation (34) is of the form of $D^n - D_0^n = K\Phi t$ to which the grain-growth curves were fitted. The exponent value of 3 that appears in Eq. (34) is satisfying since the fitting of the grain-growth curves given in Table II shows exponents close to 3. In the studies in Refs. 4, 5, 8, and 15 the exponents were also averaging 3. However this was interpreted as a deviation—due to impurities or internal stresses—from the parabolic law. The present study suggests that this is an *inherent* feature of grain growth under ion irradiation at low temperatures so that the expected value for the exponent n is 3. The cubic exponent originates from the introduction of the probability term f_{GB}. Although previous studies agreed on the idea that only atomic displacements created at the grain boundaries participate in their migration and hence in grain growth[2,5,8] no such correcting term was introduced. Without such a term, Alexander's model resulted in the prediction of the parabolic law, in disagreement with experiments.

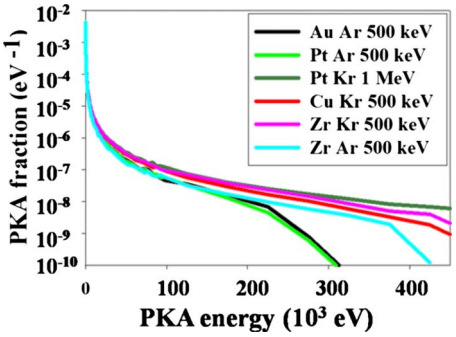

FIG. 5. (Color online) Recoil energy spectrum calculated using the PKA energy data generated by SRIM2003 for simulations running 10 000 ions for 80 nm Au foil irradiated with 500 keV Ar ions, 90 nm Cu foil irradiated with 500 keV Kr ions, 80 nm Pt foil irradiated with 1 MeV Kr ions, 80 nm Pt foil irradiated with 500 keV Ar ions, 80 nm Zr foil irradiated with 500 keV Kr ions, and 80 nm Zr foil irradiated with 500 keV Ar ions.

V. COMPARISON WITH EXPERIMENT

Given that the theoretical value of the grain-growth exponent ($n=3$) is in good agreement with experimental results, it should be possible to use Eq. (34) to correctly predict the experimentally observed grain-growth kinetics in the pure elemental thin films (Au, Pt, Zr, and Cu). To evaluate K, it is necessary to estimate the average number of thermal spikes per ion (χ) and the average thermal spike energy (Q), and the size of the average spike d_{spike}. This is done in Secs. V A and V B.

A. Estimate of the average number of thermal spikes per ion (χ) and the average thermal spike energy (Q)

When ions travel through matter, some of the PKAs generated have enough energy to trigger a collisional cascade which results in a thermal spike, while others result in isolated displacements. The latter do not need to be taken into consideration in this analysis. We therefore need to find the recoil spectra and count those which have a high enough energy to trigger a thermal spike.

SRIM2003 was used to generate the atomic recoil spectra. The software keeps track of all the recoils generated during each Monte Carlo simulation, and writes them in a large text file. A program was written to sort through the SRIM2003 outputs and collect the recoil data that generate the recoil spectra. The SRIM2003 runs were performed in full cascade mode for 10 000 ions in order to obtain good statistics. The displacement energy thresholds were taken as the default value of 25 eV/at. Figure 5 shows the recoil energy spectra for the cases of interest in this study: Au irradiated with 500 keV Ar ions, Cu irradiated with 500 keV Kr ions, Pt irradiated with 1 MeV Kr ions and 500 keV Ar ions, Zr irradiated with 500 keV Kr ions, and Zr irradiated with 500 keV Ar ions.

To determine the average number of thermal spikes created per ion (χ), and the average energy of a thermal spike Q, the following assumptions were used:

(a) We consider an energy threshold $E^a_{\text{threshold}}$ above which a PKA gives rise to a thermal spike and below which it can be disregarded. Although this recoil energy threshold for cascade formation is not known for most metals, it should depend on the incident irradiating particle, the target material and depth. Fenn-Tye and Marwick[26] evaluated it to be 5–10 keV, in their study of cascade mixing in Pd films using energetic heavy ions such as 100 keV Ne, 200 keV Ar and Kr, and 400 keV Xe. In this study, we will take the same energy threshold $E^a_{\text{threshold}}$ for all materials to be 2 keV (knowing that this may result in an underestimation of the average thermal spike energy).

(b) At the other end of the PKA energy distribution, primary recoils can be generated with energies up to hundreds of keV, depending on the ion energy and target atomic mass. However both Monte Carlo calculations and TEM studies[27] have shown that high energy cascades break up into subcascades. For instance, English and Jenkins[28] estimated that in Cu_3Au, PKAs of energy higher than 30 keV are divided into subcascades. In a study of high energy displacement cascades in Cu and Au, Proennecke[29] observed the formation of subcascades for high energy PKAs. Thus, literature suggests the existence of a second threshold energy $E^b_{\text{threshold}}$ above which a PKA will break into subcascades. Proennecke calculated this threshold energy for gold to be between 200 and 300 keV. This concept of threshold energy for subcascade formation was also supported by Rossi and Nastasi[30] who argued that for self-ion cascades, a spike composed of a single dense cascade could develop only when the kinetic energy of a recoil falls below a given critical value E_C, which was related to the mass and density of the target through empirical relationships obtained using the ZBL potential.[31] For an initial recoil energy E greater than E_C, the cascade would form $n=E/E_C$, subcascades until the collision energy in the cascade reaches the value of E_C.

In light of the above arguments, we make an estimate of the average number of thermal spikes per ion χ and the average energy Q of the thermal spikes by sorting through the outputs generated by SRIM and applying the following algorithm:

⇒If $<E_{\text{PKA}}<E^a_{\text{threshold}}$, then the PKA can be disregarded: the number of spikes generated by this PKA is $n=0$.
⇒ If $E^a_{\text{threshold}}<E_{\text{PKA}}E^b_{\text{threshold}}$, then the PKA gives rise to one spike of energy E_{PKA}: $n=1$.
⇒ If $E_{\text{PKA}}>E^b_{\text{threshold}}$, then the PKA energy is broken into $n=E_{\text{PKA}}/E^b_{\text{threshold}}$ subcascades of energy $E^b_{\text{threshold}}$.

In this study, $E^a_{\text{threshold}}$ was set to 2 keV, and $E^b_{\text{threshold}}$ was set to 200 keV. Although the above model can result in fractional subcascades (e.g., $n=1.45$ subcascades of energy $E^b_{\text{threshold}}$), it is considered to be a reasonable description of the phenomenon since it allows to take into account subcascade formation which is a general feature of energetic PKAs, while energy conservation is respected.

The number of spikes induced by each ion and the energy of the spikes were calculated according to the rules described above. When averaged over the number of ions for which the SRIM2003 runs were done (i.e., 10 000 ions), this gave the number of thermal spikes triggered by the ion X

$$X=\frac{\sum_i n_i}{N_{\text{ions}}}, \tag{35}$$

where n_i is the number of spikes triggered by ion i and N_{ions} is the total number of ions. The average number of thermal spikes triggered per ion per unit depth in the thin-film χ was then obtained by simply dividing Eq. (35) by the thickness of the slab used in the simulation.

Also, the average energy of the spikes created for a given material and a given ion type/energy could also be estimated according to

$$Q=\frac{\sum_i n_i \bar{E}_i}{\sum_i n_i}, \tag{36}$$

where $\bar{E}_i$ is the average energy of the spikes created by ion i.

B. Estimation of the average spike size

The average thermal spike energy Q obtained was then used to estimate the size of the average thermal spike. In their study of computer simulation of defect production by displacement cascades in metals, Bacon *et al.*[32] showed that the maximum size of the liquidlike region (equivalent to the thermal spike) in defect cascades of energies up to 5 keV was given by

$$d_{\text{spike}}=6a_0(Q)^{1/3}, \tag{37}$$

where d_{spike} is the diameter of the thermal spike in nanometers, a_0 is the lattice parameter of the material in nanometers, and Q is the energy of the cascade in keV. Equation (37) was found to apply for higher cascade energies as well. In studies of cascade formation in Fe[33] and in Ni_3Al[34] where cascade energies higher than 10 keV were simulated, the predicted values of d_{spike} obtained with Eq. (37) for $Q=10$ keV and 30–50 keV were close to the values found in the simulations, and the range of d_{spike} values for higher energies was entirely consistent with experimental data.[27,28] We have used this expression to estimate the size of the thermal spike at low temperatures.

C. Calculation of grain-growth curves for the experiments conducted

The parameters involved in the expression of K [in Eq. (34)] were evaluated using the values of the material properties and irradiation parameters listed in Tables III and IV, and using a generic grain-boundary width $(\delta/2)=3$ Å. The experimental data were fitted to Eq. (34) with the only variable being the activation energy for atomic jumps within a spike, E_a [or the parameter β if Eq. (31) is used]. Values of β

TABLE III. Values of material properties involved in the thermal spike model of grain growth under ion irradiation for Zr, Cu, Pt, and Au (Ref. 37).

Element	Ion type/energy	Flux (ions/cm^2-s)	$E^a_{\text{threshold}}$ (keV)	$E^b_{\text{threshold}}$ (keV)	χ	Q (keV)	d_{cas} (nm)
Zr	Kr/500 keV	2.5×10^{12}	2	200	6.51	20.3	5.3
Cu	Kr/500 keV	2.5×10^{12}	2	200	13.7	18.8	5.7
Pt	Ar/500 keV	2.5×10^{12}	2	200	5.84	13.9	5.7
	Kr/1 MeV	1.25×10^{12}	2	200	10.9	22.0	6.6
Au	Ar/500 keV	2.5×10^{12}	2	200	4.78	14.5	6.0

in ion-beam mixing experiments were found to be around 0.14.[35,36] In our case, we were able to obtain a good fit of the grain-growth curves by using the values of β in Table V. The fact that the values of β obtained for ion-beam induced grain growth are within the same order of magnitude from the ion-beam mixing experiments mentioned above is remarkable since these values were obtained from experimental data studying different phenomena.

Figure 6 shows the experimental data (i.e., average grain size evolution with ion dose) versus the data predicted by the model using the values in Tables III–V for the different elements. The grain-growth curves obtained from the model show good agreement with the experimental data bringing further validation of the model. We now discuss possible mechanisms to explain the grain-growth enhancement in the thermally assisted regime.

VI. THERMALLY ASSISTED REGIME

A. Ion-irradiation-induced grain-growth and radiation-enhanced diffusion

As reported before, for irradiation temperatures higher than a certain temperature threshold, which is in the {0.14–0.22} T_{melt} range, both grain-growth rate and the final grain size are enhanced with increasing irradiation temperature. Thermal enhancement of radiation processes is usually interpreted within the frame of the radiation-enhanced diffusion: irradiation creates additional point defects and both the higher defect concentration and the significant number of defects annihilated at sinks accelerate microstructural evolution processes. Although there is no supersaturation of point defects near grain boundaries, there could be an established defect flux from the bulk which could accelerate grain-boundary migration. In fact, at the highest temperatures, a contribution from point defect fluxes to the grain boundaries should not be excluded (especially in the sink-dominated regime). Evidence that this is the case is provided by the observation of voids decorating the grain boundaries during the irradiation of Au with 500 keV Ar ions at 573 K which, according to Fig. 2, was performed in the sink-dominated regime. As shown in Fig. 7, which presents a bright-field micrograph of the Au foil irradiated to the final dose of 10^{16} ions/cm^2, significant grain growth has occurred (compared to the initial grain size shown in Fig. 1) but voids have also formed at the grain boundaries. This indicates that for these irradiation conditions, point defects are arriving at the grain-boundary sinks in a non-negligible amount, which can affect the grain-boundary migration process. However, it should be pointed out that void formation was not observed in any of the irradiations carried out in the recombination-dominated regime which constitute most of the irradiations carried out in this study. Also, no change in grain-growth behavior was observed when the flux was changed by a factor of two, as would be expected if radiation-enhanced diffusion were to play a major role in the grain-growth process in this regime. Other researchers made similar experimental observations: grain growth was shown to be independent of the flux in Cu foils irradiated with 200 keV Ar ions at room temperature (therefore in the thermally assisted regime) after changing the ion flux by a factor of 20.[6] Atwater *et al.* also found no dependence of grain growth on flux in a study of Au films irradiated with 200 keV Xe ions at two different fluxes (different by a factor of 10).[8] This means that the grain size is a function of ion fluence rather than ion flux, which implies that the thermal enhancement of ion-irradiation-induced grain growth is not likely to be caused by a conventional radiation-enhanced diffusion process. Further careful experiments conducted specifically in recombination-dominated regime and sink-dominated regime, respectively, would be beneficial to determine the exact dependence of grain growth in the thermally assisted regime.

Since radiation-enhanced diffusion is not likely to be the reason for the grain-growth kinetic enhancement observed in the thermally assisted regime, it is possible that the temperature dependence of grain growth in this regime arises from the temperature dependence of the thermal spike process it-

TABLE IV. Irradiation parameters used to calculate K.

Element	ν Debye frequency (Hz) ($\times10^{13}$)	$\mathbf{V}_{\text{at}}$ atomic volume (cm^3) ($\times10^{-23}$)	κ_0 Thermal conductivity (eV/cm K)	c_0 Heat capacity (eV/cm^3 K) ($\times10^{19}$)	$\Delta\mathbf{H}_{\text{coh}}$ cohesive energy (eV/atom)
Zr	3.80	2.34	1.44×10^{18}	1.12	6.25
Cu	4.48	1.18	2.50×10^{19}	2.15	3.49
Pt	3.14	1.51	4.50×10^{18}	1.78	5.84
Au	2.16	1.69	2.00×10^{19}	1.56	3.81

TABLE V. Value of the parameter scaling the activation energy for atomic jumps within cascades to the cohesive energy of the material.

Material	β
Zr	0.12
Cu	0.08
Pt	0.06
Au	0.03

self (i.e., the size of the thermal spike, and the η term). Although literature is scarce on this topic, studies published to date give some evidence that this is a plausible mechanism.[32–34,38–42]

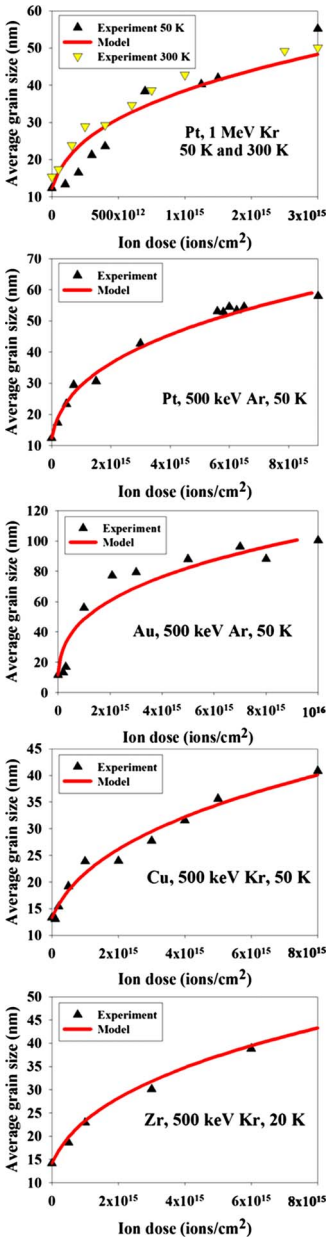

FIG. 6. (Color online) Average grain size vs ion dose. Experimental data vs model in the temperature-independent regime. Pt irradiated with Ar 500 keV ions at 298 K; Pt irradiated with 1 MeV Kr ions at 50 K and 298 K; Zr irradiated with 500 keV Kr ions at 20 K; Cu irradiated with 500 keV Kr ions at 50 K; and Au irradiated with 500 keV Ar ions at 50 K.

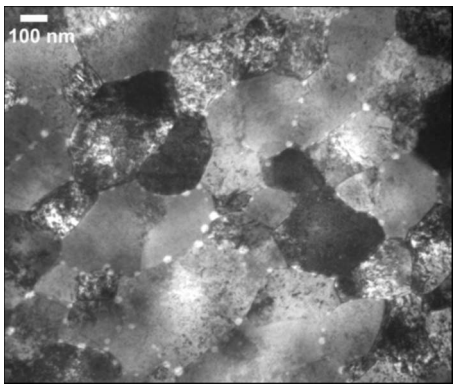

FIG. 7. Bright-field image of a Au foil irradiated at 573 K with 500 keV Ar ions to a final fluence of 10^{16} ions/cm^2 showing the formation of faceted voids decorating the grain boundaries.

B. Effect of T_{irr} on d_{spike}

Hsieh *et al.*[43] performed MD simulations of 3 keV displacement cascades in Cu and found that most atomic displacements occurred in the quasimolten core region that develops at $t \sim 0.5$ ps and persists for a few picoseconds. The mixing was found to increase modestly at 300 K compared to 0 K, and to increase more rapidly at higher substrate temperatures. As the ambient temperature of the lattice increased (T_{irr}=0, 300, 500, and 700 K), the size and the lifetime of the "quasimolten" region (spike) also increased. Also, Gao and Bacon[41] performed MD simulations of cascades in α-Fe [42] and Ni_3Al. For α-Fe,[42] simulations of 2 or 5 keV cascades were performed at 100, 400, 600, and 900 K. For the same PKA energy, the size of the thermal spike was larger at the lattice temperature of 600 K than at 100 K. In the case of Ni_3Al,[41] the results of the MD simulations were consistent with those obtained for Fe, i.e., the total number of atomic jumps within the thermal spike increased with higher substrate temperature, and the maximum size d_{spike} of the melted zone was larger at 900 K than at 100 K. At 900 K (which approximately half of the melting point of Ni_3Al) d_{spike} was found to be 1.4 times the size at 100 K. Rossi and Nastasi[30] used the results of the MD study in Ref. 43 to derive an empirical relationship between the size of the spike d_{spike} and T_{irr} of the type

$$d_{spike}(T_{irr}) = d_{spike}^{0K}\left[1 + \lambda \exp\left(-\frac{T_s}{T_{irr}}\right)\right], \tag{38}$$

where λ is a constant depending on the spike energy, the cohesive energy, and the thermal properties of the substrate, T_{irr} the initial substrate temperature, and T_s a characteristic temperature which depends on the target. For Cu, the values found for $d_{spike}^{0\ K}$, T_s, and λ are 1.6 nm, 617 K, and 1.95, respectively, with a correlation coefficient of 1. In the model proposed in this work, a larger spike size implies a higher grain-growth rate as per Eq. (32).

C. Effect of T_{irr} on η

That higher irradiation temperatures result in higher number of atomic jumps within the thermal spikes was verified by the MD simulations mentioned above. However it is

TABLE VI. Parameters for the determination of E.

Material/foil thickness (nm)	V_{at} (cm^3/atom) ($\times 10^{-23}$)	K_{iv_0} (cm^{-2}) ($\times 10^{16}$)	$\mathbf{E_v^m}$ (eV/at)	Ion type/ flux (ions/cm^2.s)	K_0 (dpa/s)	D_0 (cm)	Initial $\mathbf{k_{GB}^2}$ (cm^{-2})	$4K_0K_{iv_0}/k_{iGB}^2 \cdot k_{vGB}^2$
Zr 80	2.34	4.42	1.4[a]	Kr 500 keV 2.5×10^{12}	0.0213	1.45×10^{-6}	2.74×10^{13}	5.03×10^{-12}
Cu 90	1.18	6.98	0.71,[b] 0.82,[c] 0.9[d]	Kr 500 keV 2.5×10^{12}	0.0232	1.55×10^{-6}	2.40×10^{13}	1.13×10^{-11}
Pt 80	1.51	5.92	1.45[b] 1.35[d]	Kr^{++} 1 MeV 1.25×10^{12}	0.0185	1.35×10^{-6}	3.16×10^{13}	4.39×10^{-12}
				Ar 500 keV 2.5×10^{12}	0.0128			3.04×10^{-12}
Au 80	1.69	5.48	0.83,[b] 0.71,[c] 0.85[d]	Ar 500 keV 2.5×10^{12}	0.0119	1.50×10^{-6}	2.56×10^{13}	4.01×10^{-12}

[a]Reference 45.
[b]Reference 46.
[c]Reference 47.
[d]Reference 48.

not possible to derive an analytical expression for this increase in the parameter η in this study. Indeed, the derivation of η (presented in the previous section) depends on the obtention of the temperature distribution within the thermal spike $T(r,t)$ by solving the heat conduction equation. The analytical solution of this equation is only possible if one assumes the substrate temperature T_{irr} to be null. Thus, a higher number of jumps in the spike at higher substrate temperatures would also increase the grain-growth rate as per Eq. (32), although it is not possible to obtain a similar analytical solution as presented here.

In summary, there is evidence of the temperature dependence of defect-cascade formation in literature, which supports the idea that the temperature dependence observed in the thermally assisted regime is the direct reflection of the temperature dependence of the cascade formation process itself. Therefore, it is proposed that the enhanced grain growth under ion irradiation in the thermally assisted regime is primary caused by thermal spike size increase, and the effect on η. At the highest temperatures (especially in the sink-dominated regime) point defect fluxes to the grain boundaries may also contribute.

VII. CONCLUSIONS

A model of grain growth under ion irradiation in the temperature-independent regime was developed, based on the direct impact of irradiation-induced thermal spikes on grain boundaries. The model describes grain growth driven solely by the reduction in grain-boundary area. Grain-boundary migration occurs by atomic jumps within the thermal spikes hitting the grain boundary and biased by the local grain-boundary curvature driving force. In contrast with previous models of grain growth under ion irradiation, this model incorporates features such as subcascade formation, and the probability of subcascades occurring at grain boundaries. The model yields a power law expression relating the average grain size with the ion dose, with an inherent exponent of 3 in good agreement with experiments. In the thermally assisted regime, the increase in grain-growth rate and final grain size is explained within the framework of the same model, by the increased thermal spike size and the increase in atomic jumps within thermal spikes with higher substrate temperature. At the highest temperatures, other effects such as point defect migration to sinks may also enhance the process.

ACKNOWLEDGMENTS

Stimulating discussions with Z.-K. Liu, M. Jenkins, R. Schaeublin, and R. Averback are gratefully acknowledged. The experimental part of this research was conducted in the IVEM-Accelerator facility at Argonne National Laboratory, which was supported as a User Facility by the U.S. Department of Energy, Basic Energy Sciences, under Contract No. W-31-109-ENG-38. The expert help of P. Baldo, L. Funk, A. Liu, A. McCormick and E. Ryan was essential to the completion of the experimental part of this work. This study was funded by DOE Nuclear Engineering Education Research program under Contract No. DOE-NEER DE-FG07-01ID14115.

APPENDIX: EVALUATION OF THE REGIME OF POINT DEFECT ANNIHILATION

For nanocrystalline thin films, the sink strength for dislocations and voids is low since these were not observed on bright-field micrographs. Instead, the main sinks for defects are the free surfaces of the foil and the grain boundaries. In fact, in nanocrystalline materials, grain boundaries are likely to occupy more than 50% of the volume, unlike usual coarse-grained alloys. For calculation simplicity, these sinks are homogenized over the foil. In nanocrystalline materials, the two free surfaces can be considered as the collection of grain boundaries, respectively, of the top layer and the bottom layer of grains. Therefore if we consider grain boundaries as perfect sinks, the sink strength of free surfaces is already taken into account in the grain-boundary sink strength term. Thus, in the case where only grain-boundary sinks are considered, E is written as

$$E = \frac{4K_0K_{iv}}{k_{iGB}^2 D_i k_{vGB}^2 D_v} = \frac{4K_0K_{iv_0}}{k_{iGB}^2 k_{vGB}^2}\left(\frac{1}{D_i}+\frac{1}{D_v}\right). \quad \text{(A1)}$$

It is well known that interstitials tend to move much faster than vacancies in crystals hence $D_i \gg D_v$ so that the parameter E can be rewritten as

$$E \approx \frac{4K_0K_{iv_0}}{k_{iGB}^2 k_{vGB}^2}\frac{1}{D_v}. \quad \text{(A2)}$$

In Eq. (A2), K_{iv_0} is determined by the irradiation experimental conditions (irradiating particle flux and displacement cross sections obtained from SRIM2003 reported in Table I).

The complex expression for the grain-boundary sink strength k_{GB}^2 derived by Bullough *et al.*[44] simplifies when sinks in the bulk of grains (e.g., voids, dislocations) are negligible compared to the density of grain boundaries; k_{gb}^2 can then be expressed as

$$k_{gb}^2 \approx \frac{14.4}{R^2}. \quad \text{(A3)}$$

In order to estimate E, k_{GB}^2 was evaluated at the beginning of the irradiation when grains are smaller and k_{GB}^2 is the highest. The diffusion coefficient for vacancies is defined as

$$D_v = D_{v_0} \exp\left(-\frac{E_v^m}{k_B T}\right), \quad \text{(A4)}$$

where E_v^m is the activation energy for vacancy migration. Values of E_v^m found in literature for the different elements are reported in the table below and range from 0.7 to 1.45 eV/atom. The generic value of 10^{-2} cm^2/s was used for D_{v_0}. Table VI summarizes the values of parameters which are relevant to the determination of E. Using these values E is plotted versus irradiating temperature for the different systems: Au irradiated with 500 keV Ar ions, Cu 500 keV Kr, Pt 1 MeV Kr, and Zr 500 keV Kr.

[1] P. Wang, D. A. Thompson, and W. Smeltzer, Nucl. Instrum. Methods Phys. Res. B **16**, 288 (1986).
[2] D. E. Alexander and G. S. Was, Phys. Rev. B **47**, 2983 (1993).
[3] D. E. Alexander, G. S. Was, and L. E. Rehn, J. Appl. Phys. **70**, 1252 (1991).
[4] D. E. Alexander, G. S. Was, and L. E. Rehn, Nucl. Instrum. Methods Phys. Res. B **59-60**, 462 (1991).
[5] J. C. Liu, Ph.D. thesis, Cornell University, 1989.
[6] J. C. Liu, J. Li, and J. W. Mayer, J. Appl. Phys. **67**, 2354 (1990).
[7] J. C. Liu, M. Nastasi, and J. W. Mayer, J. Appl. Phys. **62**, 423 (1987).
[8] H. A. Atwater, C. V. Thompson, and H. I. Smith, J. Appl. Phys. **64**, 2337 (1988).
[9] A. T. Motta, A. Paesano, Jr., R. C. Birtcher, S. R. Teixeira, and L. Amaral, Nucl. Instrum. Methods Phys. Res. B **175-177**, 521 (2001).
[10] D. Kaoumi, A. Motta, and R. C. Birtcher, Nucl. Instrum. Methods Phys. Res. B **242**, 490 (2006).
[11] P. Wang, D. A. Thompson, and W. Smeltzer, Nucl. Instrum. Methods Phys. Res. B **7-8**, 97 (1985).
[12] G. H. Vineyard, Radiat. Eff. **29**, 245 (1976).
[13] G. J. Dienes and G. H. Vineyard, *Radiation Effects in Solids* (Interscience, New York, 1957).
[14] W. L. Johnson, Y. T. Cheng, M. Van Rossum, and M.-A. Nicolet, Nucl. Instrum. Methods Phys. Res. B **7-8**, 657 (1985).
[15] D. E. Alexander and G. S. Was, Surf. Coat. Technol. **51**, 333 (1992).
[16] R. A. Andrievski, J. Mater. Sci. **38**, 1367 (2003).
[17] C. Suryanarayana, J. Mater. Chem. **54**, 24 (2002).
[18] H. Gleiter, Acta Mater. **48**, 1 (2000).
[19] D. Kaoumi, A. T. Motta, and R. C. Birtcher, J. ASTM Int. **4**, JAI100743 (2007).
[20] C. W. Allen and E. A. Ryan, Proceedings of the Materials Research Society Fall Meeting, **439**, 277 (1997).
[21] J. Ziegler, J. P. Biersack, and U. Littmark, *The Stopping and Range of Ions in Matter* (Pergamon, New York, 1985).
[22] H. V. Atkinson, Acta Metall. **36**, 469 (1988).
[23] S. K. Kurtz and F. M. A. Carpay, J. Appl. Phys. **51**, 5726 (1980).
[24] M. Hillert, Acta Metall. **13**, 227 (1965).
[25] W. Voegeli, K. Albe, and H. Hahn, Nucl. Instrum. Methods Phys. Res. B **202**, 230 (2003).
[26] I. A. Fenn-Tye and A. D. Marwick, Nucl. Instrum. Methods Phys. Res. B **18**, 236 (1986).
[27] M. L. Jenkins and C. A. English, J. Nucl. Mater. **108-109**, 46 (1982).
[28] C. A. English and M. L. Jenkins, J. Nucl. Mater. **96**, 341 (1981).
[29] S. Proennecke, Ph.D. thesis, Ecole Polytechnique Federale de Lausanne, 1992.
[30] F. Rossi and M. Nastasi, J. Appl. Phys. **69**, 1310 (1991).
[31] F. Rossi, D. M. Parkin, and M. Nastasi, J. Mater. Res. **4**, 137 (1989).
[32] D. J. Bacon, A. F. Calder, F. Gao, V. G. Kapinos, and S. J. Wooding, Nucl. Instrum. Methods Phys. Res. B **102**, 37 (1995).
[33] F. Gao, S. J. Wooding, D. J. Bacon, A. F. Calder, and L. M. Howe, Proceedings of the Materials Research Society Fall Meeting, **439**, 395 (1997).
[34] D. J. Bacon, F. Gao, and Y. N. Osetsky, J. Nucl. Mater. **276**, 1 (2000).
[35] W. L. Johnson, Y. T. Cheng, M. Van Rossum, and M. A. Nicolet, Nucl. Instrum. Methods Phys. Res. B **7-8**, 657 (1985).
[36] M. V. Rossum and Y. T. Cheng, Diffus. Defect Data, Pt. A **A57–A58**, 1 (1988).
[37] C. Kittel, *Introduction to Solid State Physics*, 6th ed. (Wiley, New York, 1986).
[38] T. Diaz de la Rubia, R. S. Averback, R. Benedek, and W. E. King, Phys. Rev. Lett. **59**, 1930 (1987).
[39] T. Diaz de la Rubia, R. S. Averback, H. Horngming, and R. Benedek, J. Mater. Res. **4**, 579 (1989).
[40] D. J. Bacon, F. Gao, and N. O. Yu, J. Comput.-Aided Mater. Des. **6**, 225 (1999).
[41] F. Gao and D. J. Bacon, Philos. Mag. A **80**, 1453 (2000).
[42] F. Gao, D. J. Bacon, P. E. J. Flewitt, and T. A. Lewis, J. Nucl. Mater. **249**, 77 (1997).
[43] H. Hsieh, T. Diaz de la Rubia, R. S. Averback, and R. Benedek, Phys. Rev. B **40**, 9986 (1989).
[44] R. Bullough, M. R. Hayns, and M. H. Wood, J. Nucl. Mater. **90**, 44 (1980).
[45] G. M. Hood, J. Nucl. Mater. **139**, 179 (1986).
[46] E. A. Brandes, *Smithells Metals Reference Book*, 7th ed. (Butterworth-Heinemann, Boston, 1998).
[47] N. Q. Lam, L. Dagens, and N. V. Doan, J. Phys. F: Met. Phys. **13**, 2503 (1983).
[48] M. I. Baskes and C. F. Melius, Phys. Rev. B **20**, 3197 (1979).